ELSEVIER

Journal of Structural Geology 29 (2007) 1855–1869

JOURNAL OF STRUCTURAL GEOLOGY

www.elsevier.com/locate/jsg

Amorphous material formed by the mechanochemical effect in natural pseudotachylyte of crushing origin: A case study of the Iida-Matsukawa Fault, Nagano Prefecture, Central Japan

Kana Ozawa*, Shigeru Takizawa

Division of Earth Evolution Sciences, Graduate School of Life and Environmental Sciences, University of Tsukuba, Tennodai 1-1-1, Tsukuba, Ibaraki 305-8572, Japan

Received 23 June 2006; received in revised form 23 August 2007; accepted 24 August 2007
Available online 22 September 2007

Abstract

Pseudotachylytes from the Iida-Matsukawa Fault, Central Japan (Iida pseudotachylytes), are described down to the nanometer scale using high-resolution electron microscopy, scanning electron microscopy, analyses of chemical compositions, and mercury intrusion porosimetry. The pseudotachylyte matrix chiefly consists of nanoscale particles and elongated submicron fragments with biotite composition; amorphous material of several tens of nanometers in size is also observed, despite the absence of melt textures. Lattice fringe images reveal that the amorphous phase coexists with lattice distortion in deformed biotite fragments that are several hundreds of nanometers in size. The presence of these submicrostructures indicates that the amorphous material formed by mechanical stress during the comminution process; that is, via the ''mechanochemical effect.'' We conclude that amorphous material does not always provide evidence of the rapid cooling of melt in pseudotachylyte. The amorphous materials present in the Iida pseudotachylyte resulted from the mechanochemical effect due to both shear stress and normal stress during the comminution process that accompanied fault motion.
© 2007 Elsevier Ltd. All rights reserved.

Keywords: Amorphous material; Crush-origin pseudotachylyte; Mechanochemical effect; High-resolution electron microscopy

1. Introduction

Pseudotachylytes are fault rocks that are generally thought to form by frictional fusion and comminution during paleoseismic fault movements (e.g. Philpotts, 1964; Sibson, 1975; Allen, 1979). Although it has been debated in the past as to whether pseudotachylyte matrix originates from frictional fusion or comminution (Wenk, 1978), the controversy was resolved by Spray's (1995) experimental study undertaken using friction welding apparatus, which demonstrated that comminution is a necessary precursor to frictional melting.

Pseudotachylytes are now generally divided into melt-origin types and crush-origin types. Melt-origin types contain melt textures such as glass or glassy material, spherulites, dendritic microlites, vesicles, amygdules, rounded and embayed clasts, and sulfide blebs (e.g. Philpotts, 1964; Sibson, 1975; Allen, 1979; Maddock, 1983, 1986; Maddock et al., 1987; Magloughlin, 1989, 1992, 2005; Lin, 1994, 1999). Melt-origin pseudotachylytes from the Fuyun Fault zone, China, have a largely glassy matrix that is nearly isotropic and variable in color from colorless to grey, brown, and yellowish-brown, as well as containing flow streaks (Lin, 1994).

In contrast, crush-origin types show none of these melt textures. Such pseudotachylytes have been described from the Iida-Matsukawa Fault, Japan (Lin et al., 1994; Lin, 1996, 1997b), the Nojima Fault, Japan (Shigetomi and Lin, 1999; Lin et al., 2001), and the Shimotsuburai Fault (Kano et al., 2004), part of the active fault system of the Itoigawa-Shizuoka Tectonic Line, Japan.

Glass and other amorphous material are known to form not only via the rapid cooling of melt, but also by alteration (e.g.

* Corresponding author.
E-mail address: kanaoz@arsia.geo.tsukuba.ac.jp (K. Ozawa).

0191-8141/$ - see front matter © 2007 Elsevier Ltd. All rights reserved.
doi:10.1016/j.jsg.2007.08.008

Henley and Ellis, 1983) and comminution (e.g. Kubo, 1963; Kubo and Miyazaki, 1968; Kieffer et al., 1976; Lin and Nadiv, 1979; Sakabe et al., 1998). The results of rotary shear sliding experiments using samples of granite and quartzite have shown that the amorphous silica formed by comminution on a sliding surface can be observed by transmission electron microscopy (TEM) (Yund et al., 1990). Most recently, Goldsby and Tullis (2002) and Di Toro et al. (2004) reported an extraordinary progressive reduction in frictional resistance upon sliding surfaces under wet conditions at subseismic slip rates. The authors explained this weakening as resulting from amorphization and the formation of gel via shearing and comminution in the presence of water, and suggested this to be one of the weakening mechanisms of faults during seismic slip.

The above experimental studies clearly show that the presence of amorphous material formed by comminution is an essential factor in understanding fault strength and faulting processes during earthquakes; however, the presence of amorphous material formed by comminution has yet been reported from natural fault rocks.

The present study describes submicron-scale textures observed via electron microscopy and comminution-origin amorphous material revealed by TEM analyses of crush-origin pseudotachylyte from the Iida-Matsukawa Fault, southern Nagano Prefecture, Central Japan (Iida pseudotachylyte). We propose that the amorphous material within the Iida pseudotachylyte formed via mechanochemical effects rather than rapid cooling of the melt during seismic faulting.

2. Sample locality

The Iida-Matsukawa Fault strikes NW–SE and dips 75–85° to the SW, extending for 12 km in the southern part of the Kiso Range, Central Japan (Fig. 1). Geological and topographical evidence indicates that the fault is an active sinistral strike-slip fault with a component of normal dip-slip displacement, having a horizontal slip rate of 1 mm/y (Lin et al., 2000).

Lin et al. (1994, 1996, 1997a,b) described in detail the field occurrence of pseudotachylytes and cataclastic rocks from along the Iida-Matsukawa Fault. The zone of fractured rock along the fault generally ranges in width from several meters to several tens of meters, and consists of cataclastic rocks such as cataclasite, foliated cataclasite, fault breccia, fault gouge, and pseudotachylyte (Lin, 1996, 1997a,b). The pseudotachylyte veins observed along the fault are several millimeters to several centimeters wide, dark brown to black in color (Fig. 2b), locally show a vitreous luster, and occur both as simple veins along the main fault plane (fault veins) and as complex networks of veins (injection veins; Fig. 2a) within host granitic cataclasite (Lin et al., 1994; Lin, 1996, 1997a,b).

The granitic cataclasite, the host rock of the pseudotachylyte, occurs along the main fault plane in a zone that ranges in width from several tens of centimeters to several tens of meters (Lin et al., 1994). The host rock is largely composed of quartz, feldspar, and biotite (Lin, 1997a). In places, the cataclasite contains a well-developed foliation that dips at 25–35° to the SE, subparallel to the main fault plane. The

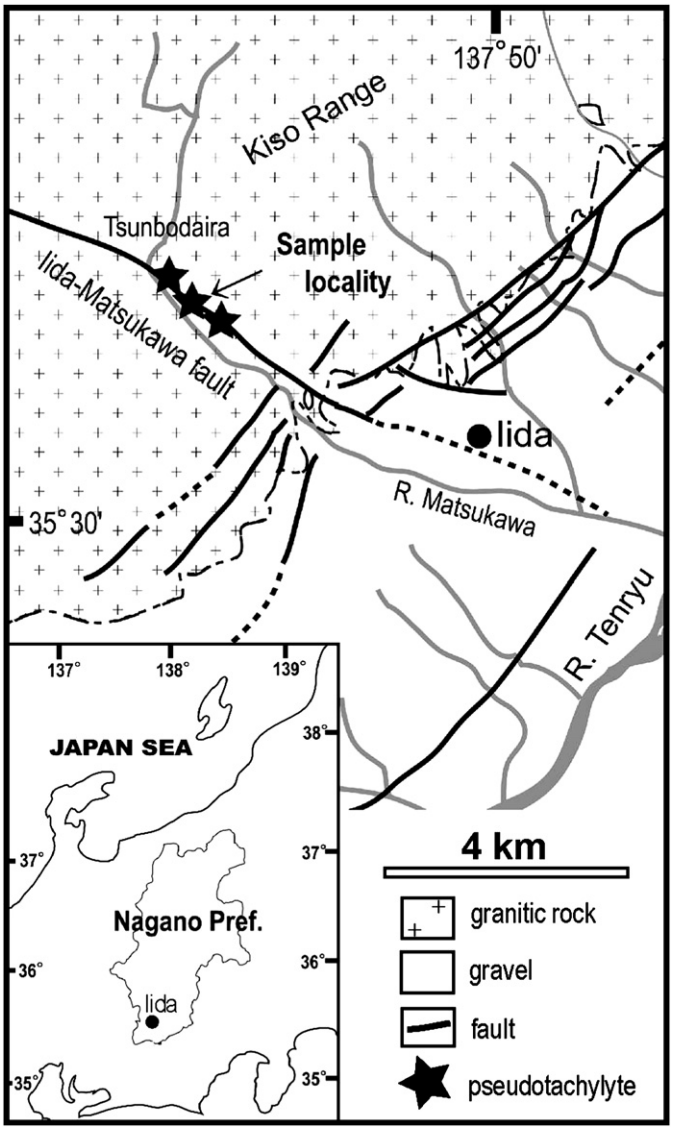

Fig. 1. Index map and simplified geological map of the Iida region, southern Nagano Prefecture, Central Japan (modified from Lin, 1996).

foliation is defined by the preferred orientation of biotite clasts and aggregates of quartz grains and feldspar porphyroclasts. Deformed biotite in the cataclasite shows cleavage steps, mica ''fish'' geometries, and kink bands, indicating a sinistral sense of shear (Lin, 1996, 1997a; Lin et al., 2000).

The pseudotachylyte analyzed in the present study was collected from a fault vein in an outcrop that corresponds to Location 2 of Lin et al. (1994) and Lin (1996), located along the central segment of the Iida-Matsukawa Fault at the southernmost part of Tsunbodaira, along the Matsukawa River in Iida City (Fig. 1).

3. Analytical methods

Microstructures in the pseudotachylyte were observed using a JEOL JSM-6320F high-resolution scanning electron microscope (HRSEM) with an accelerating voltage of 5 kV, a JEOL JEM-100CX TEM with an accelerating voltage of

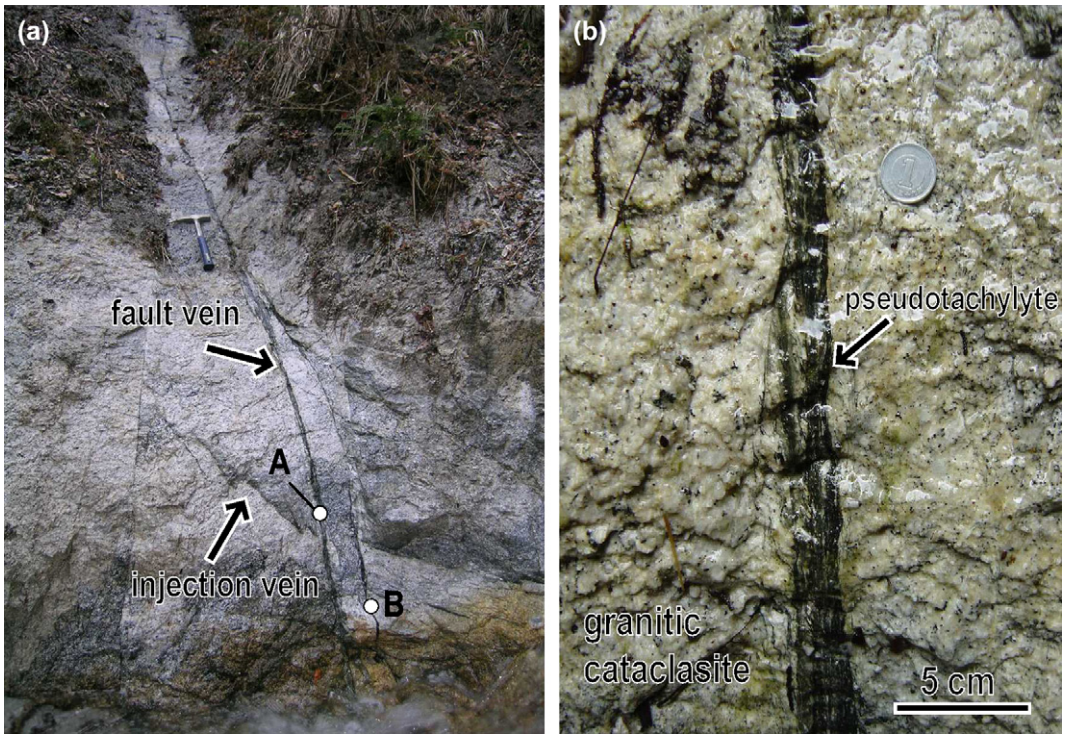

Fig. 2. Photographs of the field occurrence of Iida pseudotachylyte. (a) Pseudotachylyte occurring as black veins (arrow). The location of this outcrop is shown in Fig. 1. White circles indicate sampling points for XRF-EDS analyses. (b) Pseudotachylyte and granitic cataclasite.

100 kV, and a JEOL JEM-2100 high-resolution transmission electron microscope (HRTEM) with an accelerating voltage of 200 kV. The freeze-dried breakage surface of the pseudotachylyte was investigated by HRSEM. Foils for TEM observations of microstructures in the pseudotachylyte were prepared from thin sections, without epoxy resin, using an ion-beam. Samples for HRSEM and TEM observations of particles smaller than 2 μm were prepared as follows. Untreated lumps of the pseudotachylyte were suspended in distilled water using ultrasonic agitation; the <2 μm fractions were then selected by hydraulic elutriation. The suspension was again dispersed with ultrasonic agitation, then dropped onto an aluminum tape subjected to hydrophilic treatment for HRSEM observations of the shapes and surface textures of fragments within the pseudotachylyte. The same suspension was dropped onto a microgrid (without films) subjected to hydrophilic treatment for TEM observations. Samples for HRSEM analysis were covered with platinum, while TEM specimens were carbon-coated.

X-ray diffraction (XRD) patterns of the pseudotachylyte and host granitic rock were obtained using a RINT RAD-C X-ray diffractometer operated under the following analytical conditions: filtered Cu-K_α radiation, X-ray generator at 40 kV, 25 mA, scanning step 0.02°, scanning speed 2°/min, divergence slit 1°, scattering slit 1°, and receiving slit 0.15 mm. Powdered samples for XRD analysis, analyzed to *identify* clay minerals, comprised the <2 μm fractions selected by hydraulic elutriation and prepared as well-oriented aggregates on a silica glass slide. The treatments used in this study were as follows. Individual samples were heated to either 150, 350, 450, 550, or 600 °C for 1 h, followed by quenching in air and treatment with ethylene glycol.

The bulk chemical compositions of the pseudotachylyte and host rock were determined via the analysis of whole-rock powder samples using a JSX-3220 energy-dispersive X-ray fluorescence spectrometer (XRF-EDS). The powder sample of pseudotachylyte for XRF-EDS analysis was selected, as much as possible, from only black veins of pseudotachylyte, as viewed under the microscope.

The chemical composition of the pseudotachylyte matrix was determined from carbon-covered specimens, polished thin sections, and foils for TEM analysis. The thin sections were examined using a JEOL JSM-5600LV scanning electron microscope (SEM) operating at 15 kV with an energy-dispersive X-ray spectrometer (EDS). The foils for TEM analyses were examined using a JEOL JEM-2100 HRTEM with a 200 kV accelerating voltage and fitted with an EDS.

The pore-size distributions of freeze-dried specimens of the pseudotachylyte and host rock were determined using a Shimadzu-Micromeritics AutoPore IV-9520 mercury porosimeter. This method is capable of determining pore sizes ranging from 0.003 to 180 μm.

4. Microstructures

4.1. Optical observations

The pseudotachylytes investigated in this study contain angular clasts of quartz and feldspar within a dense fine-grained matrix that is pale to dark brown under plane-polarized light

(Fig. 3a, b). The boundary between the pseudotachylyte and host rock (granitic cataclasite) is generally sharp (Fig. 3a). Pseudotachylyte veins cut across deformed biotite in the host rock, which is elongated and contains kink bands (Fig. 3c, d); however, few fragments of biotite are observed in the pseudotachylyte itself. The pseudotachylyte matrix contains thin dark brown layers that resemble flow structures (Fig. 3a). The pseudotachylyte contains no melt textures such as spherulites, dendritic microlites, vesicles, amygdules, rounded and embayed clasts, and sulfide blebs.

4.2. HRSEM observations

The pseudotachylyte matrix is relatively porous, and mainly characterized by extremely fine-grained aggregates that range in size from several tens of nanometers to a few micrometers (Fig. 4a–c). Most of the larger fragments of a few micronmeters in size, are angular to subangular and irregular in shape, with sharp or little-blunt edges and peaks. The fragments show conchoidal fractures and step-like textures on the surfaces. Most of the surface features are relatively smooth, without etch pits or deep cavities (Fig. 5a–d). Some fragments contain numerous small scratches and holes upon sub-rounded surfaces (Fig. 5b).

Roundness is an estimate of the degree of smoothness of a grain surface (e.g. Leeder, 1982), and the analyzed fragments show a low degree of roundness, approximately 0.2–0.3 according to the scheme of Krumbein (1941, Plate 1). The smaller submicron fragments—several hundreds of nanometers in size—tend to have more spherical forms; however, they also have many corners on their surfaces, with relatively low roundness values of 0.3–0.4 (Fig. 5e–g). The surface textures of submicron fragments with blunt edges are slightly rough, without etch pits or deep cavities (Figs. 4b, 5e–g). The pseudotachylyte matrix does not contain melt textures such as stringy textures (e.g. Spray, 1989, 1995; Kennedy and Spray, 1992).

4.3. TEM observations

The pseudotachylyte matrix mainly consists of randomly oriented fragments that range in size from several tens of nanometers to a few micrometers; the minimum size is approximately 20 nm. The larger angular to sub-rounded fragments, which range in size from several hundreds of nanometers to a few micrometers, are generally isolated within the matrix, and supported by elongated fragments of several hundred nanometers in length and nanoscale particles smaller than 100 nm (Figs. 6a, 8a). The nanoscale particles have irregular tabular shapes (Figs. 7a, 8b), while the elongated fragments show evidence of gliding and are bent and torn along layer boundaries (Figs. 6c, 8c–e). Few euhedral particles are observed in the pseudotachylyte matrix.

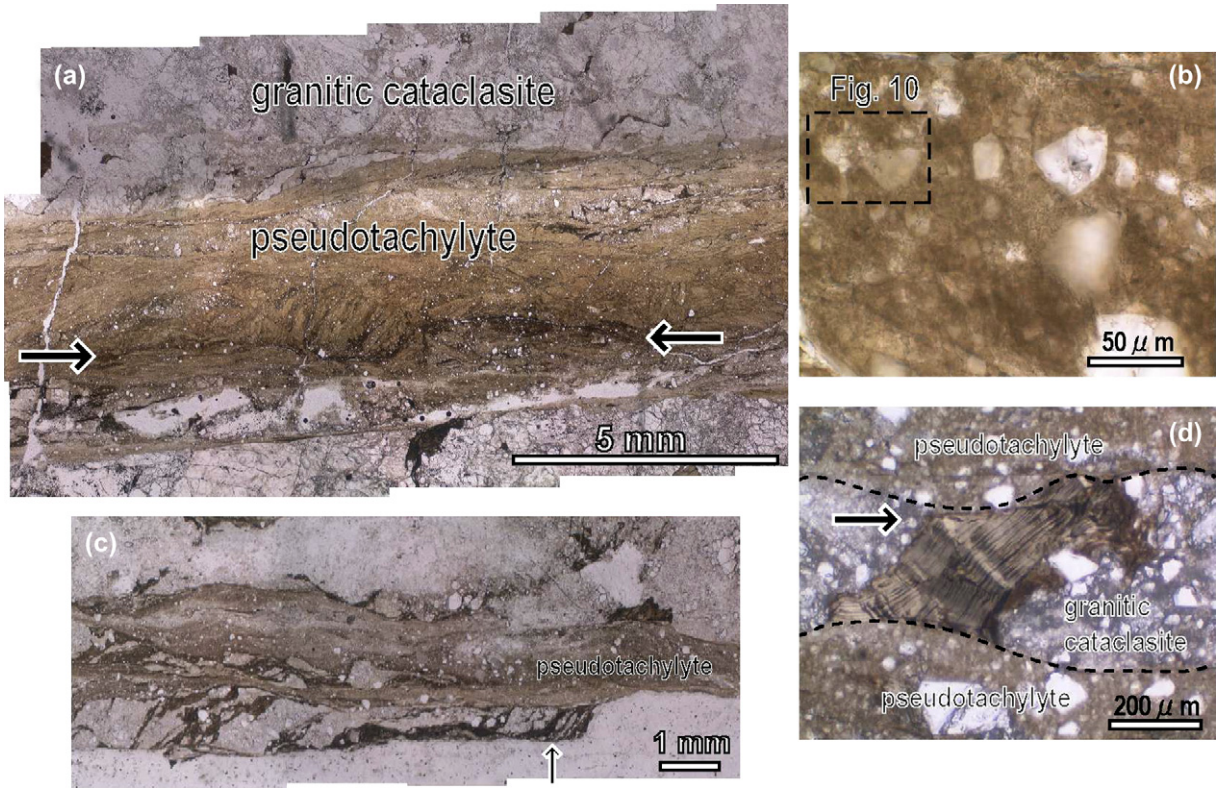

Fig. 3. Photomicrographs of the textures of Iida pseudotachylyte. (a) Thin dark brown layers with flow structures. The texture formed by fluidization (arrow). PPL. (b) Fine-grained pale brown to dark brown matrix and angular fragments of quartz and feldspar. The outlined area indicates the field of view shown in Fig. 9. PPL. (c) Dark brown layers (deformed biotite) cut by a pseudotachylyte vein. PPL. (d) Biotite with kink bands cut by a pseudotachylyte vein (arrow). PPL.

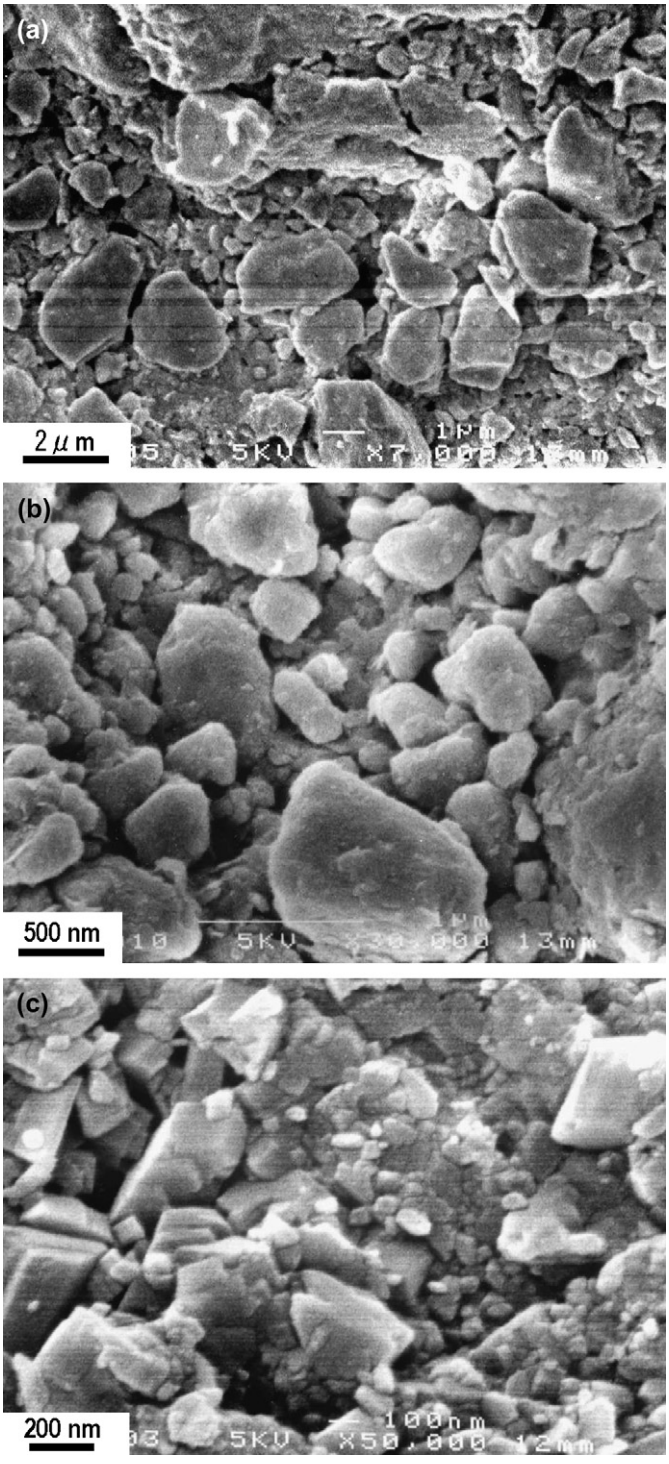

Fig. 4. HRSEM photomicrographs of textures on the breakage surfaces of Iida pseudotachylyte. (a) Angular to subangular fragments and extremely fine-grained matrix (×7000). (b) Pseudotachylyte matrix (×30,000). (c) Fragments of several tens of nanometers in size exist within the pseudotachylyte matrix (×50,000).

The selected area diffraction (SAD) patterns obtained from 100 kV TEM observations of areas dominated by the elongated fragments and nanoscale tabular particles revealed the superimposition of diffuse ring patterns, ring patterns with biotite spacings, and several diffraction spots (Fig. 6b, c). This finding indicates that amorphous material coexists with very fine crystalline fragments in such areas of the pseudotachylyte, and that the fragments are randomly orientated. The SAD patterns were taken with an aperture of 500 nm diameter due to the limitations of the technique employed by the 100 kV TEM. There is also the risk of amorphization arising from damage by the ion-beam when preparing specimens thinned by ion milling. To cope with these problems, fragments smaller than 2 μm were dispersed by ultrasonic agitation in distilled water, and the particles on the microgrids were then observed to verify the amorphous material more accurately, as shown in Fig. 7. SAD revealed that most of the angular to sub-rounded particles of several hundreds of nanometers in size have a single-crystal pattern (Fig. 7b), while agglomerations of nanoscale tabular particles show diffuse ring patterns (Fig. 7a).

Lattice fringe images of the deformed elongated fragments, as obtained using 200 kV TEM, revealed some lattice fringes with 1 nm spacings, with some of the spaces of the lattice fringes being non-periodic and indistinct (Fig. 8d–f). The above results indicate that the nanoscale tabular particles are amorphous material, whereas the deformed elongated fragments include amorphous phases and lattice distortion. The diffraction spots in the SAD patterns obtained by 100 kV TEM are probably derived from the larger grains (several hundreds of nanometers in size) adjacent to the smaller particles.

Biotite fragments were picked out of the host rock and observed by 100 kV TEM by placing them on a microgrid without a film. SAD revealed that most of the biotite fragments have single-crystal patterns (Fig. 7c).

5. X-ray diffraction patterns

The XRD patterns of the main minerals in the pseudotachylyte and host rock are shown in Fig. 9a. The pseudotachylyte consists of quartz, plagioclase, alkali feldspar, and a little clay mineral. No increased background is observed in the XRD patterns of pseudotachylyte. The host rock consists of quartz, plagioclase, alkali feldspar, and clay mineral that include mica clay minerals. The XRD patterns of the clay minerals in the pseudotachylyte and host rock are shown in Fig. 9b and c, respectively. The clay minerals were identified according to Oinuma and Kodama (1967). The 7-Å reflections in both pseudotachylyte and host rock disappeared after heating at 550 °C, suggesting kaolinite. The 10-Å reflection in the host rock did not disappear after heat treatment, suggesting mica clay minerals, while the 14-Å reflections in both the pseudotachylyte and host rock shifted to 17 Å, suggesting montmorillonite. The pseudotachylyte contains fewer clay minerals than the host rock. Of note, the peaks of mica clay minerals were identified only in the host rock, not in the pseudotachylyte.

6. Chemical composition

Table 1 shows the bulk chemical compositions of the pseudotachylytes and host rock analyzed by XRF-EDS. Sampling points for the XRF-EDS analyses are shown in Fig. 2a. The

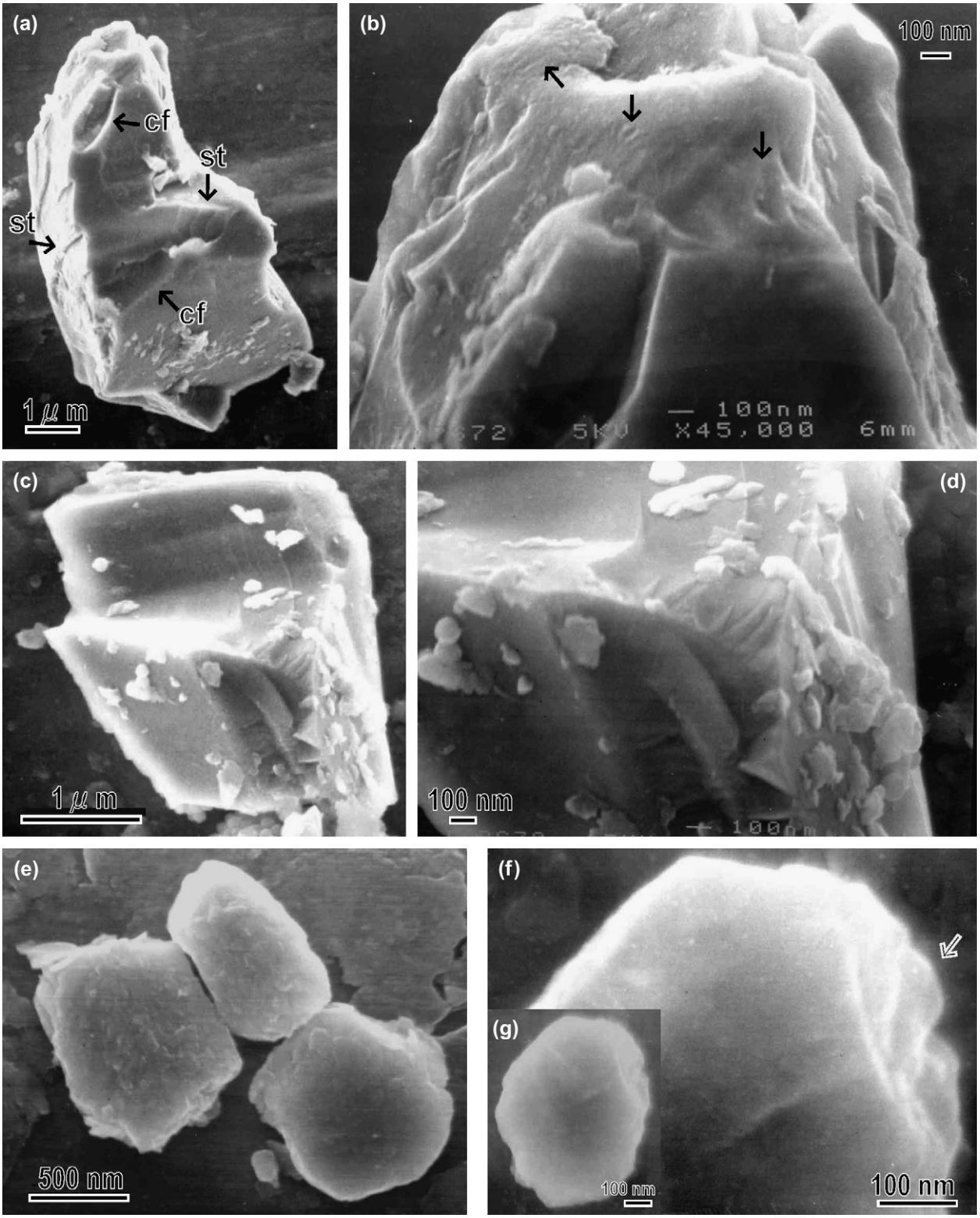

Fig. 5. HRSEM photomicrographs of the surface textures of fragments <1 μm. (a) Angular fragment with conchoidal fractures (cf) and step-like textures (st). (b) Enlargement of the upper part of the fragment shown in (a). Arrows highlight many small scratches and holes. (c) Conchoidal fracture. (d) Step-like textures upon a conchoidal fracture surface. Enlargement of the central part of the fragment shown in (c). (e) Submicron fragments with relatively rounded shapes and slightly rough surfaces, similar to orange peel-like texture. (f) Enlargement of the upper right part of the fragment shown in (g). Submicron fragments with blunt edges similar to subconchoidal fracture (arrow).

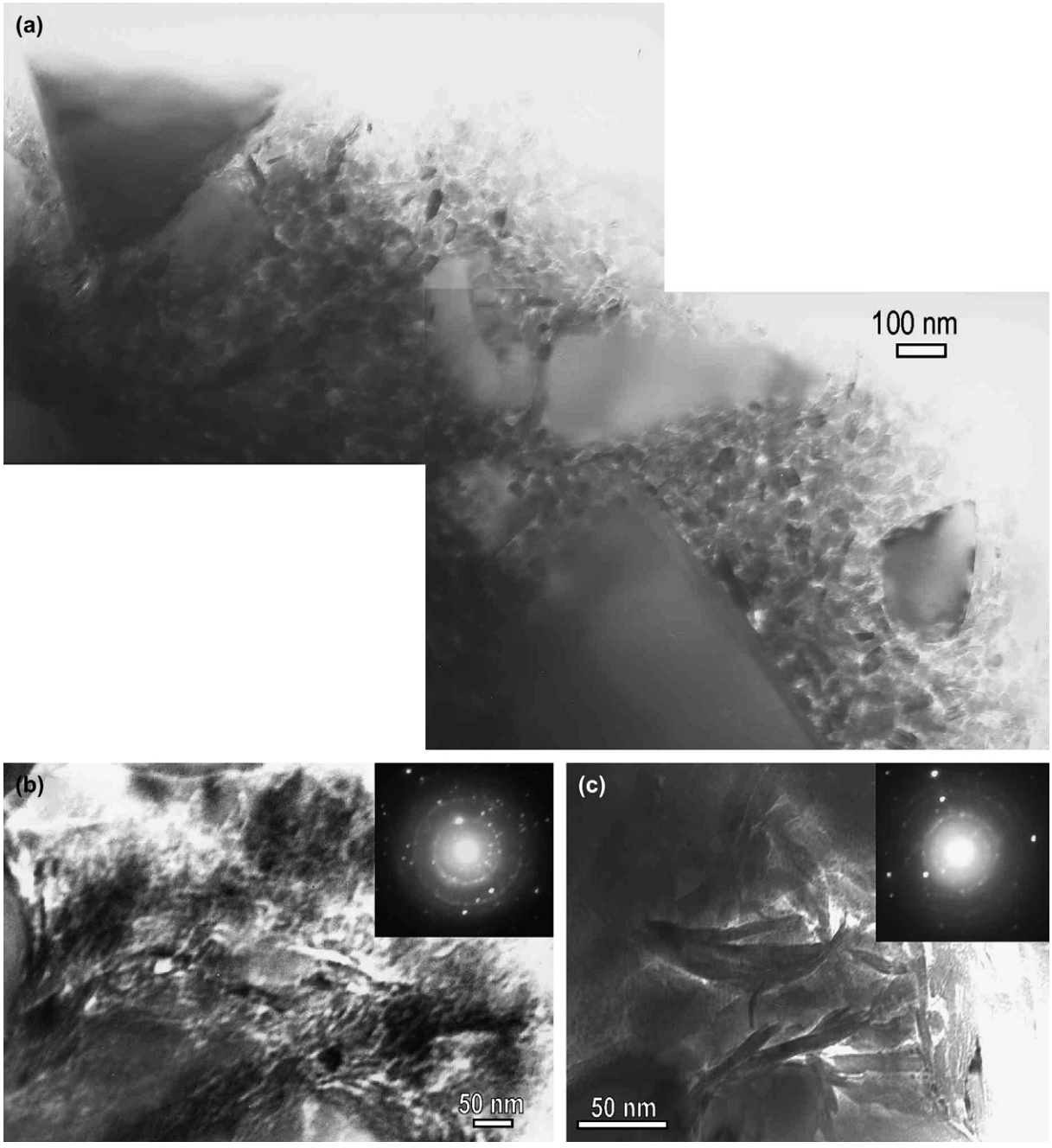

Fig. 6. TEM micrographs of bright-field (BF) images of the pseudotachylyte matrix obtained using 100 kV TEM. (a) Randomly orientated fragments that range in size from several tens of nanometers to a few micrometers. (b, c) Higher-magnification micrographs of a region of the pseudotachylyte matrix dominated by nanoscale particles smaller than 100 nm. Deformed elongated fragments are locally observed (c). Insets in (b) and (c) show the corresponding SAD patterns, showing the superimposition of diffuse ring patterns, ring patterns with biotite spacings, and diffraction spots. The SAD patterns were obtained with an aperture diameter of 500 nm.

pseudotachylytes have a slightly lower SiO_2 content and higher TiO_2, Fe_2O_3, and MgO contents than the host rock. Elemental maps obtained using SEM-EDS reveal that the pseudotachylyte matrix is particularly enriched in Mg, Ti, and Fe (Figs. 3b, 10).

The chemical compositions of particles smaller than 1 μm in the pseudotachylyte matrix were analyzed using TEM-EDS. Both the elongated fragments and the nanoscale tabular particles consist of Mg, Al, Si, K, Ti, and Fe. The C peaks detected by TEM-EDS analysis reflect contamination from the carbon coating (Fig. 11a, b).

7. Pore-size distribution

The results of pore-size analyses are shown in Fig. 12. The modal pore diameters of the pseudotachylyte and host rock are 0.0098 and 0.068 μm, respectively, while the total intrusion volumes are 0.026 and 0.040 ml/g. The porosity of the

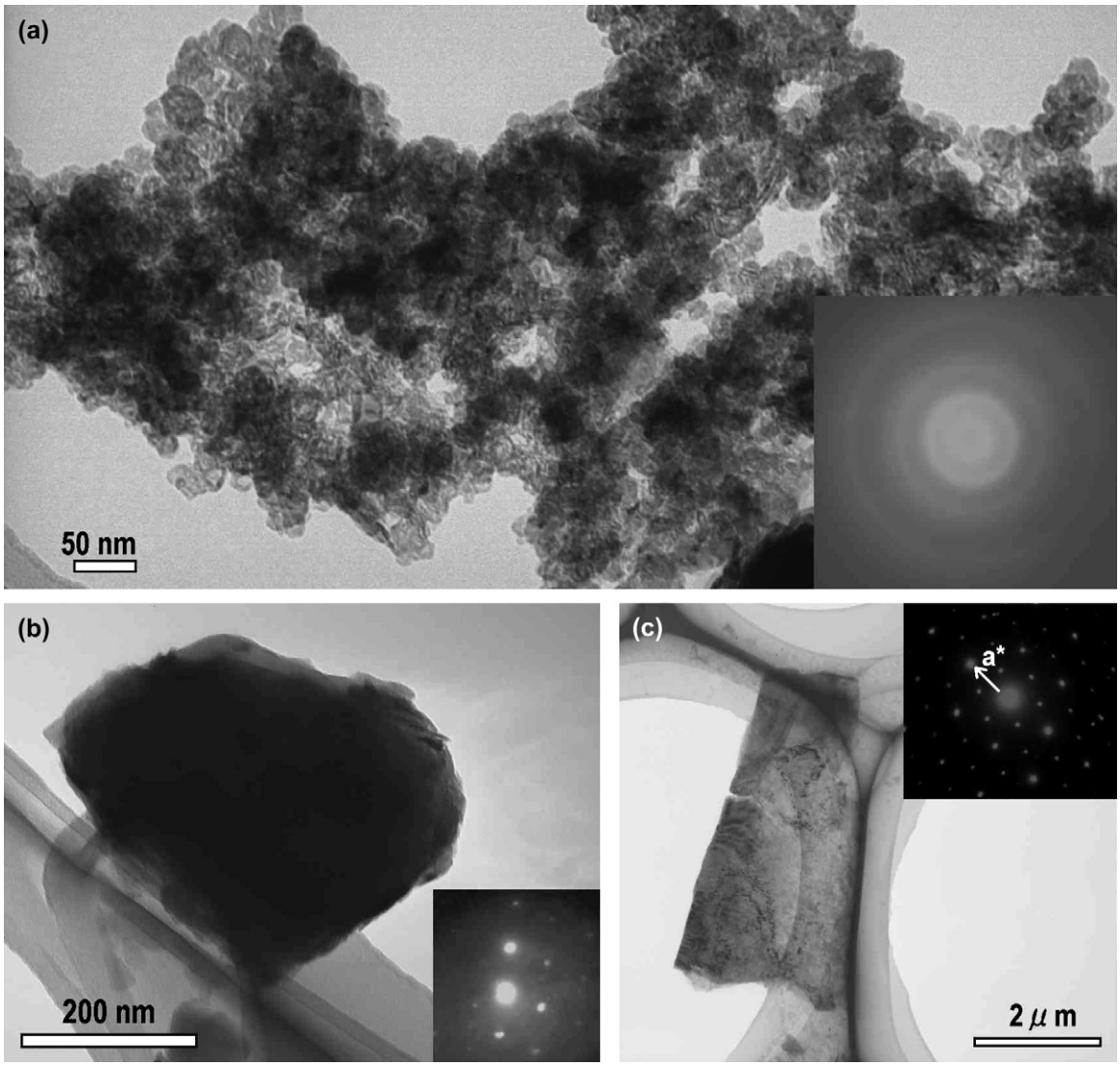

Fig. 7. TEM micrographs of the particles of <1 μm in size in the pseudotachylyte matrix that were dispersed with ultrasonic agitation. (a) Agglomeration of nanoscale tabular particles. The inset shows the corresponding SAD pattern, which demonstrates diffuse ring patterns, indicating amorphous material. (b) Sub-rounded of several hundreds of nanometers in size show a single-crystal pattern by SAD. (c) TEM micrographs showing a BF image and SAD pattern of a biotite fragment sampled from the host rock. All SAD patterns were obtained with a diameter aperture of 500 nm.

pseudotachylyte is 6.4%, whereas that of the host rock is 9.6%. These data clearly demonstrate that the host rock is more porous than the pseudotachylyte.

8. Discussion

8.1. Evidence for crush-origin pseudotachylyte

Based on optical microscopy and SEM observations, Lin et al. (1994, 1996) reported that pseudotachylytes from the Iida-Matsukawa Fault contain few melt textures, and that the matrix mainly consists of fine-grained angular fragments larger than 2–3 μm, indicating an origin via crushing rather than melting. Our own optical microscopy and HRSEM observations also reveal the absence of melt textures such as spherulites, dendritic microlites, vesicles, amygdules, sulfide blebs, and stringy textures.

Previous studies have reported the results of SEM observations of quartz grains within granitic rocks subjected to triaxial compression tests (e.g. Krinsley and Doornkamp, 1973; Dengler, 1976; Kanaori et al., 1980, 1982). These studies described quartz grains with angular shapes and sharp edges and peaks, exhibiting conchoidal fractures and step-like textures on the surfaces.

The fragments of a few micrometers in size in the Iida pseudotachylyte also show conchoidal fractures and step-like textures (Fig. 5a–c), indicating an origin via crushing; however, some of their edges and peaks are rounded (Fig. 5b), and the submicron fragments tend to be spherical in shape (Fig. 5e–g). Such rounded fragments have been documented to form not only by melting but also by attrition wear (e.g. Chester et al., 1993, 2003) and chemical dissolution in groundwater (e.g. Kanaori et al., 1980, 1982; Kanaori, 1983). Chester et al. (1993) suggested that rounded fragments in ultracataclasites

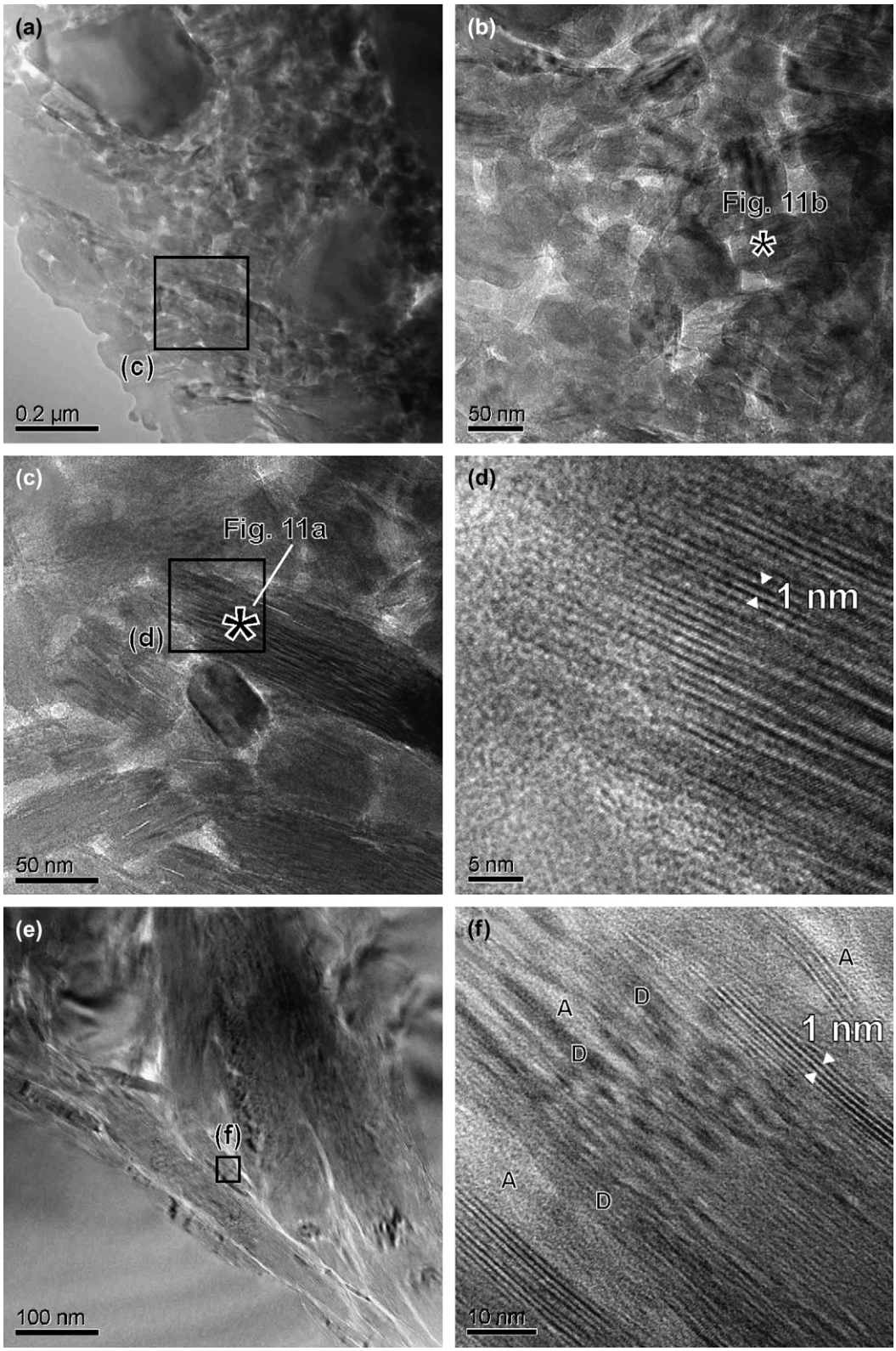

Fig. 8. HRTEM micrographs of the pseudotachylyte matrix. (a) BF image of the pseudotachylyte matrix. The outlined area indicates the field of view shown in (c). (b, c) BF images of an area consisting of nanoscale tabular particles with irregular shapes and elongated fragments. Asterisks represent the sites of qualitative EDS analyses (see Fig. 11). Both fragments have biotite compositions. (d) Lattice fringe image of the area outlined in (c). (e) Bent and fractured elongated fragment. (f) Lattice fringe image of the area outlined in (e). Periodic lattice fringes with 1 nm spacing, corresponding to the (001) spacing of biotite, are indistinct and appear to lack periodicity, indicating lattice distortion (D) and the presence of an amorphous phase (A).

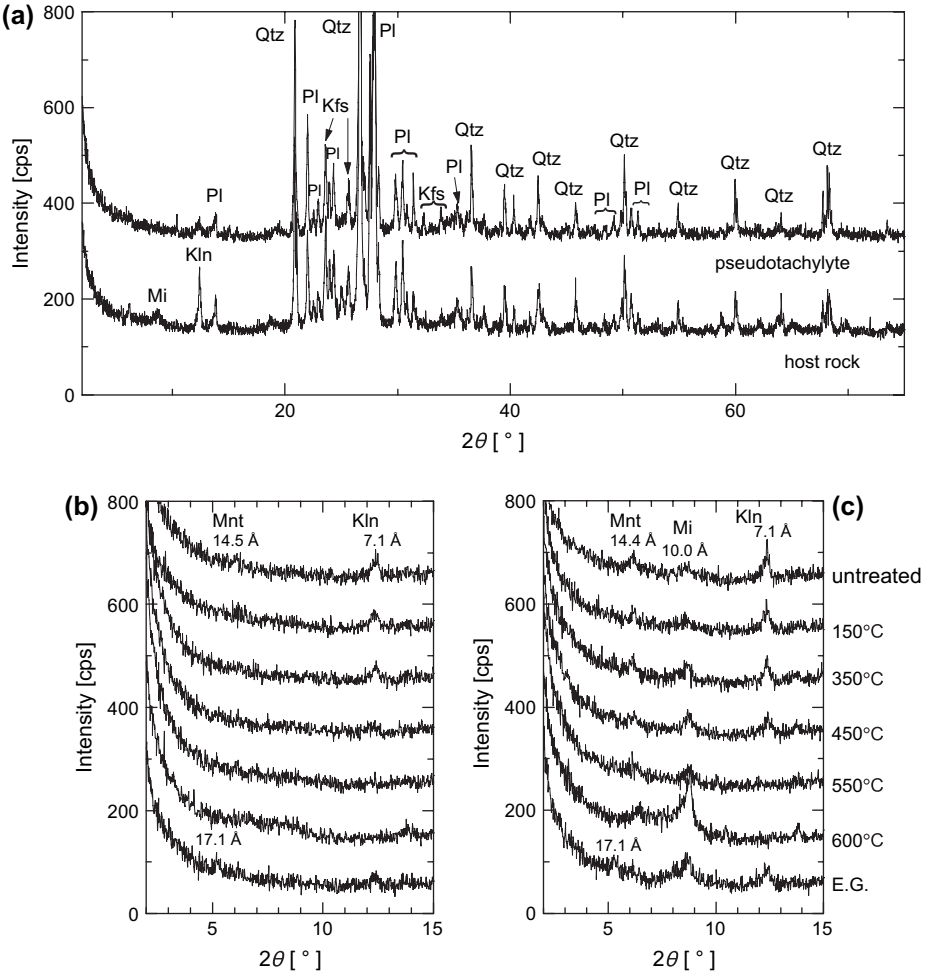

Fig. 9. X-ray diffraction patterns of pseudotachylyte and host rock (granitic cataclasite). (a) Spectra of the main minerals. (b, c) Spectra of clay minerals detected in the hydraulically elutriated samples. (b) Pseudotachylyte. (c) Host rock: 150, 350, 450, 550, and 600 °C: heated at the given temperature for 1 h. E.G., treated with ethylene glicol; Qtz, quartz; Pl, plagioclase; Kfs, K-feldspar; Mnt, montmorillonite; Mi, mica clay mineral; Kln, kaolinite.

along the North Branch San Gabriel and Punchbowl faults formed via attrition wear as angular fragments rolled within the surrounding matrix. The shapes of particles of clay minerals and quartz, formed by prolonged grinding within a mechanical agate mortar, revealed to become rounded by TEM observations (e.g. Takahashi, 1959; Shimazu, 1962).

Table 1
Bulk compositions of host rock and pseudotachylyte, as determined by XRF-EDS

wt.%	Host rock	Pseudotachylytes			
		A-1	A-2	B-1	B-2
SiO_2	73.14	68.83	68.84	68.60	68.69
TiO_2	0.15	0.57	0.58	0.64	0.65
Al_2O_3	13.39	13.55	13.56	13.54	13.60
Fe_2O_3	1.20	5.69	5.62	5.89	5.84
MnO	0.03	0.15	0.16	0.12	0.12
MgO	0.03	0.71	0.84	0.88	1.02
CaO	1.34	2.66	2.64	2.63	2.60
Na_2O	3.06	4.03	3.93	4.31	4.17
K_2O	7.35	3.31	3.34	2.84	2.80
P_2O_5	0.30	0.51	0.49	0.55	0.51

All values are normalized to 100% totals. The locations of sampling points are shown in Fig. 2a.

Kanaori et al. (1980, 1982, 1983) examined the surface textures of quartz grains from various fault gouges using SEM, and classified the surface textures of grains into four groups based on the degree of corrosion by groundwater. They showed that the features of the grains change gradually, with progressive corrosion, from irregular angular shapes and smooth surfaces to rounded shapes and rough undulatory surfaces with etch pits and deep cavities. Lin (1999) reported that fragments of $>10\,\mu m$ in size that formed via melting have a high degree of roundness (>0.4), whereas fragments that formed via attrition wear or chemical dissolution in groundwater have a low degree of roundness (<0.4).

The fragments in the present pseudotachylyte of a few micrometers in size and with rounded edges and peaks are marked by small scratches and holes (Fig. 5b). These textures (similar to the abrasion pits reported by Baker, 1976; Fig. 2E), in combination with their low degree of roundness (0.2–0.3), suggest that the rounded edges and peaks originated via attrition wear. The degree of roundness of the submicron particles

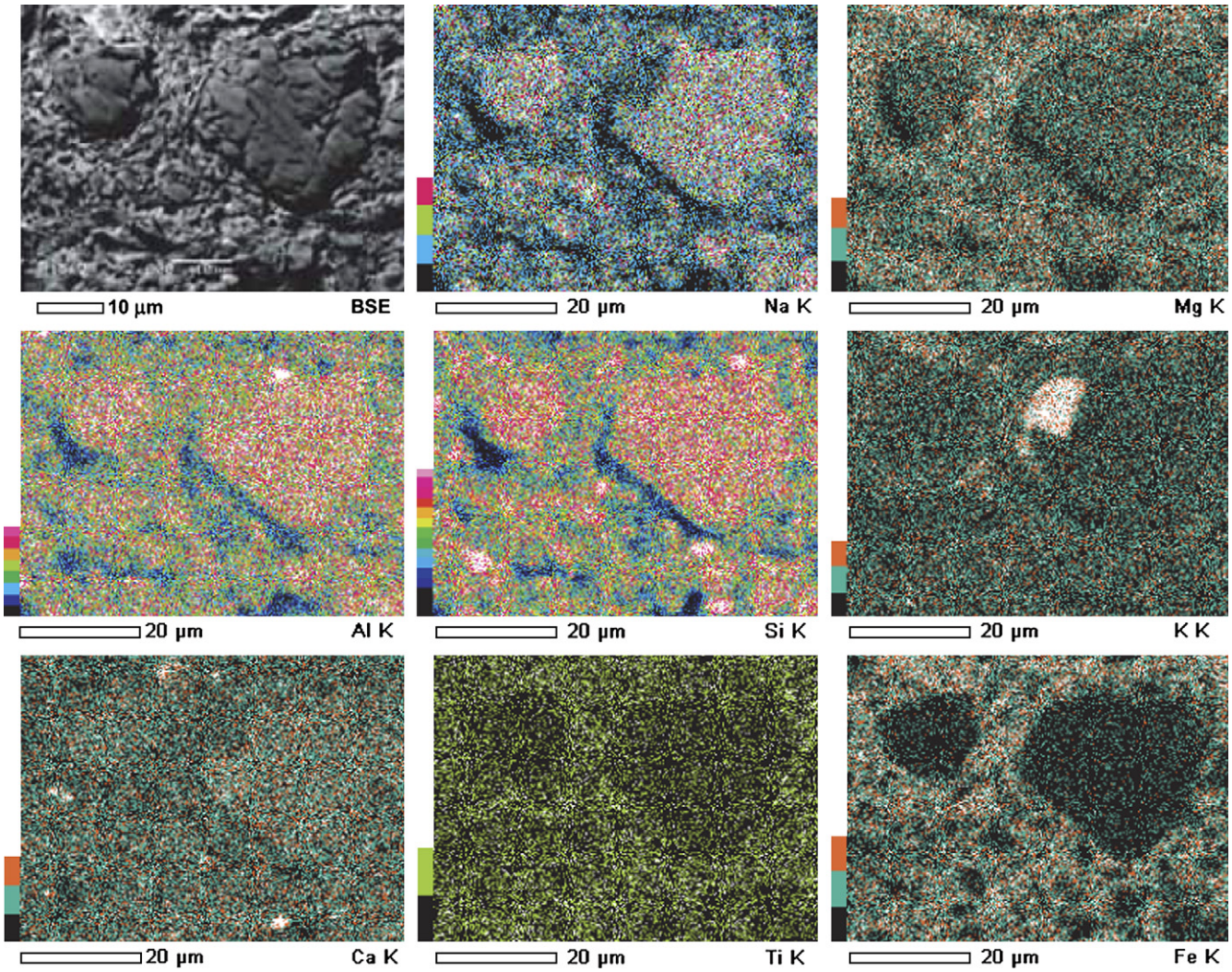

Fig. 10. Backscattered electron (BSE) micrograph and SEM-EDS elemental maps showing the distributions of Na, Mg, Al, Si, K, Ca, Ti, and Fe in the Iida pseudotachylyte. Note that the matrix is enriched in Fe, Mg, K, and Ti. BSE and mapping images were taken of the area outlined in Fig. 3b.

in the pseudotachylyte is also low (0.3–0.4), suggesting that the particles formed by processes other than melting. The submicron particles have slightly rough surfaces, without textures such as abrasion pits (Fig. 5e–g). These textures are similar to the subconchoidal fracture and orange peel-like texture formed when particles are weakly affected by chemical dissolution in groundwater following fault movement (Kanaori et al., 1980, 1982); however, the present pore-size distribution data indicate that most of the pores in the pseudotachylyte are smaller than 100 nm, and that the host rock is more porous than the pseudotachylyte (Fig. 12), thereby suggesting that fluid is unlikely to have passed through the pseudotachylyte subsequent to its formation.

The obtained XRD patterns reveal that the Iida pseudotachylyte contains fewer clay minerals than the host rock; moreover, most of the fragments have irregular shapes, and few euhedral particles were observed in the pseudotachylyte matrix. It is therefore inferred that the Iida pseudotachylyte is negligibly affected by chemical dissolution in groundwater and hydrothermal alteration subsequent to fault movement. We propose that most of the spherical submicron fragments formed by attrition wear during fault movement.

Flow structures were reported as melt textures in the melt-origin pseudotachylyte (e.g. Sibson, 1975; Berlenbach and Roering, 1992; Lin, 1994); however, they have also been reported from fluidized intrusive systems such as dikes and breccias, formed by the fluidization of solid particles (e.g. Fairbairn and Robson, 1942; Reynolds, 1954). Lin (1996, 1997b) also suggested that veins of Iida pseudotachylyte formed via the fluidization of crushed fine-grained material generated in the shear zone during seismic faulting. This interpretation was based on the similar bulk chemical compositions and grain-size distributions of injection veins and fault veins. Thus, the flow structures in the pseudotachylyte observed by optical microscope are likely to have formed by fluidization rather than the flow of a melt (Fig. 3a). On the basis of the facts presented above, we conclude that the Iida pseudotachylyte is of crush origin rather than melt origin.

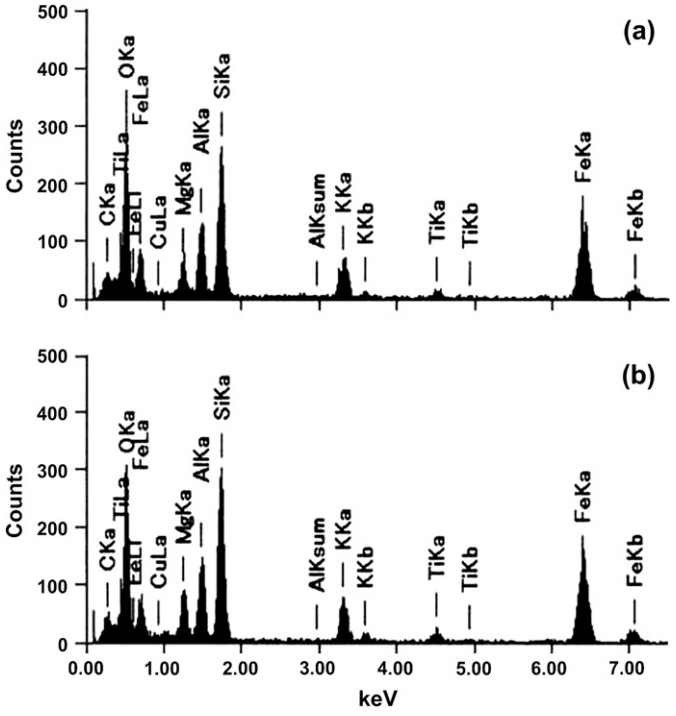

Fig. 11. TEM-EDS spectra of elongated fragments (a) and a nanoscale tabular particle (b) in the pseudotachylyte matrix. The small C peaks in both spectra are due to carbon coating. The sites of analyzed points are shown by asterisks in Fig. 8b, c.

8.2. Formation of amorphous material

Naturally occurring amorphous material can form via the rapid cooling of melt, chemical weathering, hydrothermal alteration, and mechanochemical effects induced by mechanical energy during the comminution process. We strongly favor the latter process in considering the formation of amorphous material in the Iida pseudotachylyte, as explained in the following text.

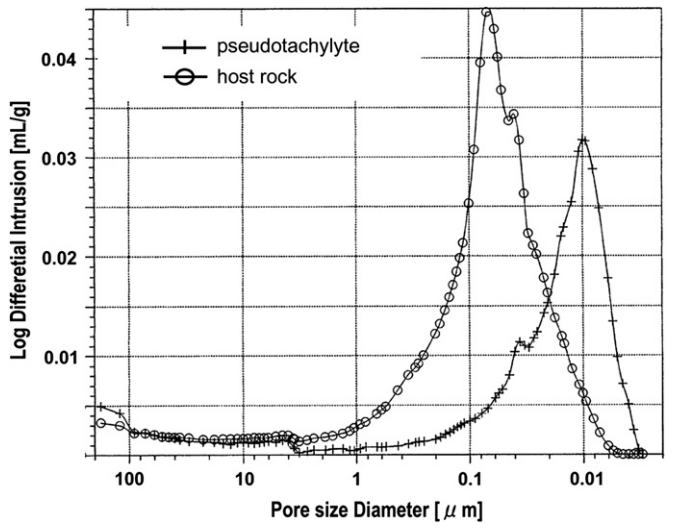

Fig. 12. Pore-size distributions of pseudotachylyte and host rock. Note that the host rock is more porous than the pseudotachylyte.

It is well known that comminution induces solid-state phase transformations such as amorphization and polymorphic transformation, as well as changes in the physical and chemical properties of materials. These phenomena are termed ‘‘mechanochemical effects’’ (e.g. Kubo, 1963; Kubo and Miyazaki, 1968; Lin and Nadiv, 1979). The driving forces of solid-state phase transformations that take place during comminution processes such as crushing, grinding, pulverizing, and polishing, include strain energy, shear energy, thermal energy, sound energy, and kinetic energy (e.g. Lin et al., 1975; Lin and Nadiv, 1979). Numerous studies report marked amorphization during the crushing or prolonged grinding of minerals, particularly quartz (e.g. Ray, 1923; De Carli and Jamieson, 1959; Shimazu, 1962; Lin and Somasundaran, 1972; Sakabe et al., 1998) and mica and clay minerals (e.g. Laws and Page, 1946; Mackenzie and Milne, 1953a,b; Yoder and Eugster, 1955; Takahashi, 1959; Perez-Rodriguez et al., 1988). Extensive work on the grinding of clay minerals has led to the proposal that the structure of crystalline parts in the material becomes disordered due to mechanical stress such as shear stress and impact stress, ultimately changing into amorphous material (e.g. Takahashi, 1959).

Yund et al. (1990) reported the formation of amorphous material via comminution in granite gouges generated experimentally by rotary shear sliding. The authors stated that the amorphous material coexisted with very fine angular crystalline fragments with irregular boundaries, and that there appeared to be a continuum between the amorphous material and crystalline fragments. In addition, the amorphous material formed by comminution was distinct from the amorphous material formed by melting, which had sharp, distinct boundaries and uniform contrast in bright-field images (e.g. Dell’ Angelo et al., 1987).

In the present study, bright-field images of the pseudotachylyte matrix obtained from 100 kV TEM analyses also indicate that the amorphous material coexists with very fine crystalline fragments that range in size from several tens to several hundreds of nanometers. As described in the earlier studies, the fragments have irregular boundaries, and there appears to be a continuum between the amorphous material and crystalline fragments (Fig. 6b).

HRTEM images of the pseudotachylyte matrix reveal that elongated fragments with 1 nm spacings, corresponding to the (001) spacing of biotite, bend or glide parallel to the layers (Fig. 8d, e), suggesting mechanical stress. The amorphous phase coexists with lattice distortion within the deformed fragments (Fig. 8e, f), indicating that the amorphous phases in the elongated fragments formed due to mechanochemical effects induced by mechanical stress.

Nanoscale amorphous material smaller than 100 nm has been reported to form during chemical weathering and the hydrothermal alteration, such as primitive clay precursors, amorphous silica, allophone, imogolite, and ferrihydrite (e.g. Tazaki, 1986; Marumo, 1995). Tazaki’s (1986) HRTEM observations of weakly weathered feldspar revealed ultrathin amorphous material in 20–25 nm circular form, termed primitive clay precursors, on the feldspar surface. These precursors, formed by

weathering, grow on the surface of the grain, whereas the nanoscale particles of pseudotachylyte identified in the present study are scattered randomly among the submicron fragments, not on the grain surface (Figs. 4c, 6a, 8a).

In the present study, TEM observations reveal that the nanoscale particles of pseudotachylyte are 20–30 nm in size and have irregular shapes (Fig. 7a). These particles have biotite compositions (see below; Figs. 8b, 11b), clearly indicating that they are not amorphous silica, allophone, imogolite, or ferrihydrite. Moreover, this pseudotachylyte is negligibly affected by hydrothermal alteration and chemical weathering following fault movement, as discussed above. For these reasons, we suggest that the nanoscale amorphous material in the pseudotachylyte formed by comminution rather than hydrothermal alteration and chemical weathering following fault movement.

The SiO_2 content of the Iida pseudotachylyte, as determined by XRF-EDS, indicates a granitic source rock. Lin (1996) also reported similar average bulk chemical compositions for the Iida pseudotachylyte and host rock, as determined using XRF, and suggested that the pseudotachylyte formed from the granitic host rock, which consists primarily of quartz, feldspar, and biotite (Lin, 1997a). In the present study, XRF-EDS analyses revealed slightly different bulk chemical compositions for the pseudotachylyte and host rock, as described above. Given that the pseudotachylyte veins cut deformed biotite in the host rock (Fig. 3c, d), and that biotite is rich in TiO_2, Fe_2O_3, and MgO, we assume that the discrepancy in bulk chemical composition reflects differences in the biotite contents of the pseudotachylyte and host rock. XRF-EDS analyses also reveal that the pseudotachylyte is likely to contain more biotite than the host rock, and that the compositions of the elongated fragments and nanoscale tabular particles in the pseudotachylyte matrix, which consist of Mg, Al, Si, K, Ti, and Fe, are biotite compositions (Figs. 8a,b, 11).

SEM-EDS analyses reveal that the pseudotachylyte matrix consists primarily of biotite composition (Fig. 10); however, peaks for mica clay minerals were not detected in the XRD patterns of the analyzed pseudotachylyte (Fig. 8). Lin (1996, 1997b) also reported the absence of XRD peaks for mica clay minerals that formed by hydrothermal alteration; however, the Iida pseudotachylyte is only weakly affected by hydrothermal alteration after fault movement (see above). We suggest that the absence of peaks for mica clay minerals in the Iida pseudotachylyte probably reflects the amorphization of biotite during the comminution process.

The amorphous material reported by Yund et al. (1990) from granite gouges produced by rotary shear sliding experiments has a feldspathic composition; however, the granite sample used in these earlier experiments was homogeneous and mainly composed of feldspar (67%), with just 5% biotite. In contrast, the host cataclasite of the Iida pseudotachylyte contains a foliation defined by the preferred orientation of biotite. The fact that the pseudotachylyte veins cut across deformed biotite in the host rock suggests that the pseudotachylyte was probably generated in the biotite-rich layers within the foliation. Shimada et al. (2004) and Toyoshima et al. (2004) reported that pseudotachylytes from the Hidaka metamorphic belt are concentrated along thin mylonitic foliation planes defined by a strong preferred orientation of micas. Accordingly, we propose that the difference between the findings of Yund et al. (1990) and the present study, in terms of the composition of amorphous material, reflects differences in the compositions of the host rocks.

XRD peaks for mica clay minerals were only detected in the host rock, not in the pseudotachylyte (Fig. 8). In addition, biotite fragments picked from the host rock are in single-crystal form (Fig. 7c), clearly suggesting that the amorphization of the biotite occurred by comminution during the formation of pseudotachylyte. Grain-size reduction by comminution is commonly attributed to wear and the attrition of quasi-static cumulative slip on the sliding surface induced by progressive shear stress (e.g. Marone and Scholz, 1989). Other recent studies have reported comminution processes attributed to dynamic rock pulverization induced by unloading–loading cycles of normal stress during the propagation of earthquake rupture (e.g. Brune, 2001; Wilson et al., 2005; Reches and Dewers, 2005). Based on the observation of a random fabric and the absence of localized slip zones, Lin et al. (1994) proposed that the Iida pseudotachylyte formed during seismic fault motion. Accordingly, we interpret that the amorphization of biotite in the Iida pseudotachylyte was induced by progressive shear stress during quasi-static slip and normal stress during dynamic rock pulverization on the sliding surface of the fault.

On the basis of rotary shear sliding experiments, Goldsby and Tullis (2002) and Di Toro et al. (2004) suggested that amorphization and the formation of gel via shearing and comminution under wet conditions is one of the weakening mechanisms of faults during seismic slip. It is therefore possible that the amorphous material in the Iida pseudotachylyte induced slip weakening during seismic slip; however, further work is required to reveal whether the amorphous material with biotite content is capable of forming a gel.

Recent studies of experimental and natural pseudotachylytes reveal that comminution is an essential precursor to frictional melting (e.g. Spray, 1995; Curewitz and Karson, 1999; Otsuki et al., 2003). During the comminution process, the activity of fragments within the pseudotachylyte increases with increasing specific surface energy and internal energy of the fragments due to grain-size reduction and the formation of lattice defects, lattice distortion, and an amorphous phase within the fragments (e.g. Kubo, 1963; Kubo and Miyazaki, 1968; Lin and Nadiv, 1979). We assume that the nanoscale to submicron fragments in the Iida pseudotachylyte are likely to have been activated, as the fragments were comminuted to the nanoscale and underwent amorphization and lattice distortion.

Many studies on the grinding of quartz, clay minerals, calcite, and metal oxides such as Fe_2O_3, TiO_2, and ZnO have reported that an increase in the activity of fragments arising from lattice distortion and amorphization during comminution acts to change their physical and chemical properties, including a lowering of the temperature of transformation, the dehydration of structural water, and increased solubility in water (e.g. Gregg et al., 1954; Burns and Bredig, 1956; Kubo, 1963;

Kubo et al., 1963; Senna et al., 1971; Lin and Somasundaran, 1972). However, the changes that occur in biotite during the comminution process remain poorly understood. Unlike crystalline materials, amorphous materials do not generally have a specific melting temperature; instead, such materials show a gradual change in melting over a wide range of temperature (e.g. Gwinn et al., 1988). To clarify the frictional melting process of pseudotachylyte, further work is required to gain an understanding of the changes in physical and chemical properties that take place during the comminution process in biotite and the melting behavior of amorphous material formed by comminution.

9. Conclusion

This study is the first to clearly document amorphous material formed by comminution, without the rapid cooling of melt, in natural crush-origin pseudotachylyte. The presence of amorphous material is therefore not always indicative of the rapid cooling of melt in pseudotachylyte. The amorphous material within the matrix of the Iida pseudotachylyte formed due to mechanochemical effects induced by shear stress and normal stress during the comminution process that accompanied fault movement.

Acknowledgements

The authors thank Prof. M. Kimata (University of Tsukuba) for his helpful suggestions. SEM-EDS, XRD, and XRF-EDS analyses were carried out at the Japan International Research Center for Agricultural Sciences (JIRCAS). HRSEM and TEM analyses were performed at the Graduate School of Comprehensive Human Sciences, University of Tsukuba. Dr. T. Hatta, Ms. S. Nemoto (JIRCAS), and Mr. Y. Ohno (University of Tsukuba) are thanked for their technical assistance. We are grateful to Mr. A. Michishita, (Shimadzu Corporation Testing & Weighing Equipment Division, Kyoto Materials Testing Center) for undertaking mercury intrusion porosimetry measurements, and Mr. A. Uchiumi, Mr. T. Suzuki, and Mr. A. Yasuhara (JEOL Ltd.) for undertaking HRTEM analyses. We thank Prof. J. Hippertt (Federal University of Ouro Preto), Prof. A. Lin (Shizuoka University), and Prof. K. O'Hara (University of Kentucky) for their reviews and kind suggestions that led to improvements in the manuscript. Dr. A. Stallard (Stallard Scientific Editing) is acknowledged for editing the final version of the manuscript.

References

Allen, A.R., 1979. Mechanism of frictional fusion in fault zones. Journal of Structural Geology 1, 231–243.

Baker, J.H.R., 1976. Environmental sensitivity of submicroscopic surface textures of quartz sand grains – a statistical evaluation. Journal of Sedimentary Petrology 46, 871–880.

Berlenbach, J.W., Roering, C., 1992. Sheath-fold-like structures in psuedotachylytes. Journal of Structural Geology 14, 847–856.

Brune, J.N., 2001. Fault normal dynamic loading and unloading: an explanation for "nongouge" rock powder and lack of fault-parallel shear bands along the San Andreas fault. 2001 Fall Meeting Abstract. EOS Transactions of American Geophysical Union 82. S22B-0655.

Burns, J.H., Bredig, M.A., 1956. Transformation of calcite to aragonite by grinding. Journal of Chemical Physics 25, 1281–1282.

Chester, F.M., Evans, J.P., Biegel, R.L., 1993. Internal structure and weakening mechanisms of the San Andreas Fault. Journal of Geophysical Research 98 (B1), 771–786.

Chester, J.S., Kronenberg, A.K., Chester, F.M., Gullemette, R.N., 2003. Characterization of natural slip surface relevant to earthquake mechanics. 2003 Fall Meeting Abstract. EOS Transactions of American Geophysical Union 84. S42C-0185.

Curewitz, D., Karson, J.A., 1999. Ultracataclasis, sintering, and frictional melting in pseudotachylytes from East Greenland. Journal of Structural Geology 21, 1693–1713.

De Carli, P.S., Jamieson, J.C., 1959. Formation of an amorphous form of quartz under shock conditions. Journal of Chemical Physics 31, 1675–1676.

Dell' Angelo, L.N., Tullis, J., Yund, R.A., 1987. Transition from dislocation creep to melt-enhanced diffusion creep in fine-grained granitic aggregate. Tectonophysics 139, 325–332.

Dengler, L., 1976. Microcracks in Crystalline Rocks. In: Wenk, H.R. (Ed.), Electron Microscopy in Mineralogy. Springer-Verlag, Berlin, New York, pp. 550–556.

Di Toro, G., Goldsby, D.L., Tullis, T.E., 2004. Friction falls towards zero in quartz rock as slip velocity approaches seismic rates. Nature 427, 436–439.

Fairbairn, H.W., Robson, G.M., 1942. Breccia at Sudbury, Ontario. Journal of Geology 50, 1–33.

Goldsby, D.L., Tullis, T.E., 2002. Low frictional strength of quartz rocks at subseismic slip rates. Geophysical Research Letters 29, doi:10.1029/2002GL015240.

Gregg, S.J., Parker, T.W., Stephens, J.M., 1954. The grinding of kaolinite. II. A more detailed study. Journal of applied chemistry 4, 666–674.

Gwinn, R.P., Norton, P.B., Goetz, P.W., 1988. The New Encyclopaedia Britannica. In: Encyclopaedia Britannica, fifteenth ed., vol. 7. Chicago.

Henley, R.W., Ellis, A.J., 1983. Geothermal systems ancient and modern: a geochemical review. Earth-Science Reviews 19, 1–50.

Kanaori, Y., Miyakoshi, K., Kakuta, T., Satake, Y., 1980. Dating fault activity by surface textures of quartz grains from fault gouges. Engineering Geology 16, 243–262.

Kanaori, Y., Miyakoshi, K., Kakuta, T., Satake, Y., 1982. Dating fault activity by surface textures of quartz grains from fault gouges (Part I). Journal of Japan Society of Engineering Geology 23, 18–32 (in Japanese, with English abstract).

Kanaori, Y., 1983. Fracturing mode analysis and relative age dating of faults by surface textures of quartz grains from fault gouges. Engineering Geology 19, 261–281.

Kano, K., Lin, A., Fukui, A., Tanaka, H., 2004. Pseudotachylytes of crushing origin from the Shimotsuburai Fault of the Itoigawa-Shizuoka Tectonic Line active fault system, Central Japan. Journal of Geological Society of Japan 110, 779–790 (in Japanese with English abstract).

Kennedy, L.A., Spray, J.G., 1992. Frictional melting of sedimentary rock during high-speed diamond drilling: an analytical SEM and TEM investigation. Tectonophysics 204, 323–337.

Kieffer, S.W., Phakey, P.P., Christie, J.M., 1976. Shock processes in porous quartzite: transmission electron microscope observation and theory. Contributions to Mineralogy and Petrology 59, 41–93.

Krinsley, D.H., Doornkamp, J.C., 1973. Atlas of Quartz Sand Surface Textures. Cambridge University Press, London.

Krumbein, W.C., 1941. Mesurement and geologic significance of shape and roundness of sedimentary particles. Journal of Sedimentary Petrology 11, 64–72.

Kubo, T., 1963. Reactivity of finely pulverized substances. Chemistry and Chemical Industry 16, 901–915 (in Japanese).

Kubo, T., Kato, M., Mitarai, M., Takahashi, J., Ohkura, K., 1963. Structural change of TiO2 and ZnO by means of mechanical grinding. Kogyo Kagaku Zasshi 66, 318–321 (in Japanese).

Kubo, T., Miyazaki, T., 1968. Mechanochemistry of inorganic substance. Journal of Chemical Society of Japan 71, 1301–1309 (in Japanese).

Laws, W.D., Page, J.B., 1946. Changes produced in kaolinite by dry grinding. Soil Science 62, 319–336.

Leeder, M.R., 1982. Sedimentology Process and Product. George Allen & Unwin Ltd., London.

Lin, A., 1994. Glassy pseudotachylyte veins from the Fuyun Fault zone, Northwest China. Journal of Structural Geology 16, 71–83.

Lin, A., Matsuda, T., Shimamoto, T., 1994. Pseudotachylyte from the Iida-Matsukawa Fault, Nagano Prefecture: pseudotachylyte of crush origin? Journal of the Tectonic Research Group of Japan 39, 51–64 (in Japanese with English abstract).

Lin, A., 1996. Injection veins of crushing-originated pseudotachylyte and fault gouge formed during seismic faulting. Engineering Geology 43, 213–224.

Lin, A., 1997a. Ductile deformation of biotite in foliated cataclasite, Iida-Matsukawa Fault, Central Japan. Journal of Asian Earth Sciences 15, 407–411.

Lin, A., 1997b. Fuluidization and rapid injection of crushed fine-grained materials in fault zones during episodes of seismic faulting. In: Zheng, et al. (Eds.), Proceedings of the 30th International Geological Congress, vol. 14. VSP, pp. 27–40.

Lin, A., 1999. Roundness of clasts in pseudotachylytes and cataclastic rocks as an indicator of frictional melting. Journal of Structural Geology 21, 473–478.

Lin, A., Matsushima, N., Maruyama, T., 2000. Late Quaternary acivity of the Iida-Matsukawa fault in the southern Ina valley, Japan. Journal of Geological Society of Japan 106, 413–425 (in Japanese, with English abstract).

Lin, A., Shimamoto, T., Maruyama, T., Shigetomi, M., Miyata, T., Takemura, K., Tanaka, H., Uda, S., Murata, A., 2001. Comparative study of cataclastic rocks from a drill core and outcrops of the Nojima Fault zone on Awaji Island, Japan. The Island Arc 10, 368–380.

Lin, I.J., Somasundaran, P., 1972. Alterlations in properties of samples during their preparation by grinding. Powder Technology 6, 171–179.

Lin, I.J., Nadiv, S., Grodzian, D.J.M., 1975. Changes in the state of solids and mechano-chemical reactions in prolonged comminution processes. Minerals Science and Engineering 7, 313–336.

Lin, I.J., Nadiv, S., 1979. Review of the phase transformation and synthesis of inorganic solids obtained by mechanical treatment (mechanochemical reactions). Material Science and Engineering 39, 193–209.

Mackenzie, R.C., Milne, A.A., 1953a. The effect of grinding on micas. Clay Minerals Bulletin 2, 57–62.

Mackenzie, R.C., Milne, A.A., 1953b. The effect of grinding on micas. I. Muscovite. Mineralogical magazine 30, 178–185.

Maddock, R.H., 1983. Melt origin of fault-generated pseudotachylytes demonstrated by textures. Geology 11, 105–108.

Maddock, R.H., 1986. Partial melting of lithic porphyroclasts in fault-generated pseudotachylytes. Neues Jahrbuch fuer Mineralogie. Abhandlungen 155, 1–14.

Maddock, R.H., Grocott, J., Van Nes, M., 1987. Vesicles, amygdales and similar structures in fault-generated pseudotachylytes. Lithos 20, 419–432.

Magloughlin, J.F., 1989. The nature and significance of pseudotachylite from the Nason terrane, North Cascade Mountains, Washington. Journal of Structural Geology 11, 907–917.

Magloughlin, J.F., 1992. Microstructural and chemical changes associated with cataclasis and frictional melting at shallow crust level: the cataclasite-pseudotachylyte connection. Tectonophysics 204, 243–260.

Magloughlin, J.F., 2005. Immiscible sulfide droplets in pseudotachylyte: Evidence for high temperature (>1200 °C) melts. Tectonophysics 402, 81–91.

Marone, C., Scholz, C.H., 1989. Particle-size distribution and microstructures within simulated fault gouge. Journal of Structural Geology 11, 799–814.

Marumo, K., 1995. Fundamental features of amorphous materials in the Earth surface. Chishitusu News 496, 11–18 (in Japanese).

Oinuma, K., Kodama, H., 1967. Use of infrared absorption spectra for identification of clay minerals in sediments. Journal of the Toyo University. General Education. Natural Science 7, 1–23.

Otsuki, K., Monzawa, N., Nagase, T., 2003. Fluidization and melting of fault gouge during seismic slip: identification in the Nojima Fault zone and implications for focal earthquake mechanisms. Journal of Geophysical Research 108 (B4), 2192, doi:10.1029/2001JB001711.

Perez-Rodriguez, J.L., Madrid Sanchez Del Villar, L., Sanchez-Soto, P.J., 1988. Effects of dry gringing on pyrophyllite. Clay Minerals 23, 399–410.

Philpotts, A.R., 1964. Origin of pseudotachylytes. American Journal of Science 262, 1008–1035.

Ray, R.C., 1923. The effect of long grinding on quartz. Proceedings of Royal Society A 102, 640–642.

Reches, Z., Dewers, T.A., 2005. Gouge formation by dynamic pulverization during earthquake rupture. Earth and Planetary Science Letters 235, 361–374.

Reynolds, D.L., 1954. Fluidization as a geological process, and its bearing on the problem of intrusive granites. American Journal of Science 252, 577–613.

Sakabe, H., Kohyama, N., Shinohara, Y., Koshi, K., 1998. Solubility in physiological solution and high-resolution TEM observation of amorphous surface layer of ground quartz particles. In: Chiyotani, K., Hosoda, Y., Aizawa, Y. (Eds.), Advances in the Prevention of Occupational Respiratory Diseases: Proceedings of the Ninth International Conference on Occupational Respiratory Diseases, Kyoto, pp. 943–947.

Senna, M., Tojo, S., Kuno, H., 1971. Polymorphic transformation of γ-Fe2O3 by isothermal ball-milling and vacuum hot-pressing. Nippon Kagaku Zasshi 92, 780–784 (in Japanese).

Shimada, K., Tanaka, H., Toyoshima, T., Obata, T., Niizato, T., 2004. Occurrence of mylonite zones and pseudotachylyte veins around the base of the upper crust: An example from the southern Hidaka metamorphic belt, Samani area, Hokkaido, Japan. Earth Planet Space 56, 1217–1223.

Shimazu, M., 1962. Structural change of silica minerals by dry mechanical grinding (I), quartz. Journal of Mineralogical Society of Japan 5, 291–310 (in Japanese).

Sibson, R.H., 1975. Generation of pseudotachylyte by ancient seismic faulting. Geophysical Journal of Royal Astronomical Society 43, 775–779.

Shigetomi, M., Lin, A., 1999. Seismic events inferred from the layering structures of fault gouge zone and pseudotachylytes in the Nojima Fault zone, Japan. Journal of Tectonic Research Group of Japan 43, 33–42 (in Japanese with English abstract).

Spray, J.G., 1989. Slickenside formation by surface melting during the mechanical excavation of rock. Journal of Structural Geology 11, 895–905.

Spray, J.G., 1995. Psedotachylyte controversy: fact or friction? Geology 23, 1119–1122.

Takahashi, H., 1959. Effects of dry grinding on kaolin minerals. I. kaolinite. Bulletin of Chemical Society of Japan 32, 235–245.

Tazaki, K., 1986. Observation of primitive clay precursors during microcline weathering. Contributions to Mineralogy and Petrology 92, 86–88.

Toyoshima, T., Obata, T., Niizato, T., Shimada, K., Komatsu, M., Wada, Y., Koyasu, T., 2004. Pseudotachylytes, related fault rocks, asperities, and crustal structures in the Hidaka metamorphic belt, Hokkaido, northern Japan. Earth Planets Space 56, 1209–1215.

Yund, R.A., Blanpied, M.L., Tullis, T.E., Weeks, J.D., 1990. Amorphous material in high strain experimental fault gouges. Journal of Geophysical Research 95, 15589–15602.

Yoder, H.S., Eugster, H.P., 1955. Synthetic and natural muscovites. Geochimica et Cosmochimica Acta 8, 225–280.

Wenk, H.R., 1978. Are psudotacylytes products of fracture or fusion? Geology 6, 507–511.

Wilson, B., Dewers, T., Reches, Z., Brune, J.N., 2005. Particle size and energetics of gouge from earthquake rupture zones. Nature 434, 749–752.